Available online at www.sciencedirect.com
SCIENCE DIRECT®
Journal of Power Sources 138 (2004) 232–239
JOURNAL OF POWER SOURCES
www.elsevier.com/locate/jpowsour

Electrochemical properties of $LiM_xCo_{1-x}O_2$ [M = Mg, Zr] prepared by sol–gel process

Hyung-Sun Kim[a], Tae-Kon Ko[a], Byung-Ki Na[b], Won Il Cho[a], Byung Won Chao[a,*]

[a] *Eco-Nano Research Center, Korea Institute of Science and Technology, Seoul 136-791, South Korea*
[b] *Division of Chemical Engineering, Chungbuk National University, Chungbuk 361-763, South Korea*

Received 2 April 2004; accepted 8 June 2004
Available online 26 August 2004

Abstract

$LiCoO_2$, Mg-doped $LiCoO_2$, and Zr doped $LiCoO_2$, are manufactured by a sol–gel method, and are used as cathode active materials for lithium rechargeable batteries. The structural characteristics of the synthesized electrodes are analyzed by X-ray diffraction. The materials have a layered structure with the space gropu $R\bar{3}m$ of hexagonal systems. $LiCoO_2$ prepared by sol–gel method shows a capacity decay over 4.3 V but $LiCoO_2$ doped with Mg and Zr give an improvement in charge–discharge cycling performance. This effect may attribute to the fact that Mg^{2+} and Zr^{4+} ions have the same size as the Li^+ ion and they locate at the inter-slab space. Therefore, they provide a pathway for the intercalation–deintercalation of Li^+ during the charge and the discharge processes and prevent distortion of the structure. Also, the formation of a solid solution on the surface of the electrode acts as the buffer to phase transition and the structure becomes very stable.

Keywords: Lithium rechargeable battery; $LiCoO_2$ cathode active material; Sol–gel method; Dopant; Magnesuim; Zirconium

1. Introduction

Cathode materials for lithium rechargeable batteries must be chemically stable to the electrolyte and must be reversible during the repeated charge–discharge process. Also, they must have high specific energy and the volume change must be very small during cycling. Li_xCoO_2, Li_xNiO_2, $Li_xMn_2O_4$, and $LiNi_xCo_xO_2$ are transition metals that satisfy these conditions. $LiCoO_2$ is mainly used as the cathode material for lithium rechargeable batteries because it is very easy to synthesize, the change in potential is very small during discharge, and the electrical conductivity is excellent.

In addition, $LiCoO_2$ has many advantages such as high discharge capacity, high specific energy, high power density, low self-discharge, and good reversibility during charge and discharge [1–4]. $LiCoO_2$ that is made by a solid-state reaction exhibits excellent properties as a cathode material. Therefore, it was selected as the cathode material for first-generation lithium-ion batteries.

$LiCoO_2$ does, however, have some disadvantages. Metallic cobalt is very expensive and toxic. Degradation of the crystal structure occurs due to the dislocation of lattice oxygen at high temperatures and overcharge to 4.2 V [5]. This structural instability results in restricted cycling performance. Therefore, the addition of dopants or the surface modification of $LiCoO_2$ has been studied to prevent fading of the discharge capacity [6–13]. For example, $A1_2O_3$ [6], SnO_2 [7], MgO [8] and ZrO_2 [9] have been coated on $LiCoO_2$ powder. These coating materials form a solid solution at the surface and provide a pathway for Li intercdation–deintercalation. They act as a buffer to phase transition. The cation dopants of nickel [10], manganese [11], aluminum [12] and boron [13] have been studied recently. Such cation doping is found to improve cycling performance, but it lowers the discharge capacity compared with bare-$LiCoO_2$. Mladenov et al. [14] have reported that magnesium doping improves both the cycling stability and the discharge capacity of $LiCoO_2$ material.

* Corresponding author. Tel.: +82-2-958-5222; fax: +82 2 958 5229.
E-mail addresses: kimhs@kist.re.kr (H.-S. Kim), bwcho@kist.re.kr (B.W. Chao).

0378-7753/$ – see front matter © 2004 Elsevier B.V. All rights reserved.
doi:10.1016/j.jpowsour.2004.06.024

In this study, $LiCoO_2$, Mg-doped $LiCoO_2$, and Zr-doped $LiCoO_2$ materials are prepared by the sol–gel method. These cation dopants are selected because their size are similar to that of Li^+ ions. The structure and the electrochemical characteristics of powders are analyzed.

2. Experimental

2.1. Synthesis of $LiCoO_2$

Lithium acetate dihydrate ($Li(CH_3COO)\cdot 2H_2O$, 98%) was used as the precursor of lithium and cobalt(II) acetate tetrahydrate($(CH_3CO_2)_2Co\cdot 4H_2O$, 99%) was used as the precursor of cobalt. The advantage of the materials is that they do not react easily with the moisture in the air.

Equal moles of lithium acetate and cobalt acetate were dissolved in distilled water. Acrylic acid was used as a chelating agent to control the reaction rate during the hydrolysis and gel reaction. The mole ratio of acrylic acid (R) was calculated as follows:

$$R = \frac{\text{the site number of metallic salt}}{\text{the number of metallic salt}} \quad (1)$$

The R of acrylic acid was 2. When the lithium salt and the cobalt salt were 1 M each, 4 M acrylic acid was required.

The mixed sol was transferred to a rotary evaporator. It was evaporated at 80 °C and 60 rpm for 3–4 h to obtain the gel precursor. An aspirator was used to reduce the reaction time under vacuum. The precursor was heated at 100 °C to obtain the gel powder. It was calcined at 500 °C under air, and calcined again at 700–900 °C to obtain a pure $LiCoO_2$ crystal with the layered structure. The above procedure is presented in Fig. 1.

2.2. Synthesis of $LiM_xCo_{1-x}O_2$ (M= Mg, Zr)

Magnesium acetate tetrahydrate ($(CH_3COO)_2Mg\cdot 4H_2O$, 99%) or zirconium(IV) acetate hydroxide ($(CH_3CO_2)_x Zr(OH)_y$, $x + y \approx 4$) were used as the starting materials for cation substitution of $LiCoCO_2$ synthesis by sol–gel method. 0.01, 0.05 or 0.1 M of additives were added for the synthesis.

Lithium acetate, cobalt acetate, and zirconium acetate (or magnesium acetate) at a ratio of $1:1-x:x$ (x = 0.01, 0.05 or 0.1) were dissolved in distilled water. Four moles of acrylic acid was added as the chelating agent to control the reaction rate of hydrolysis and the gel reaction. The mixed sol was transferred to the rotary evaporator. It was evaporated at 80 °C and 60 rpm for 3–4 h to obtain the gel precursor. An aspirator was used to reduce the reaction time under vacuum. The gel precursor was heated at 100 °C to obtain the gel powder. It was calcined at 500 °C under air, and calcined again at 800–900 °C to obtain $LiM_xCo_{1-x}O_2$. The above procedure is presented in Fig. 2.

2.3. Analysis of synthesized material

X-ray diffraction analysis (XRD; Rigaku, RINT/DMAS-2500) with Cu Kα radiation was used to determine the crystal structure of the synthesized materials. The scan range was 3°–80° with a scan step of 0.02° and a scan speed of 10° per min. Thermogravimetric analysis (TGA) was used to determine the weight loss up to 900 °C.

When a lithium ion is inserted into the active material, the electron must move simultaneously. The velocity of the electron movement inside the particle is relatively fast, but the velocity of the electron between particles is slow. The addition of a conductive material such as a carbon particle (KS-6)

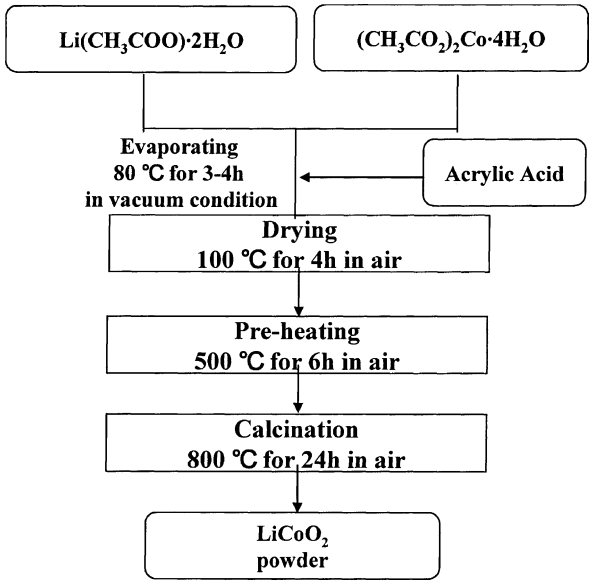

Fig. 1. Experimental procedure for synthesis of $LiCoO_2$ powder by sol–gel process.

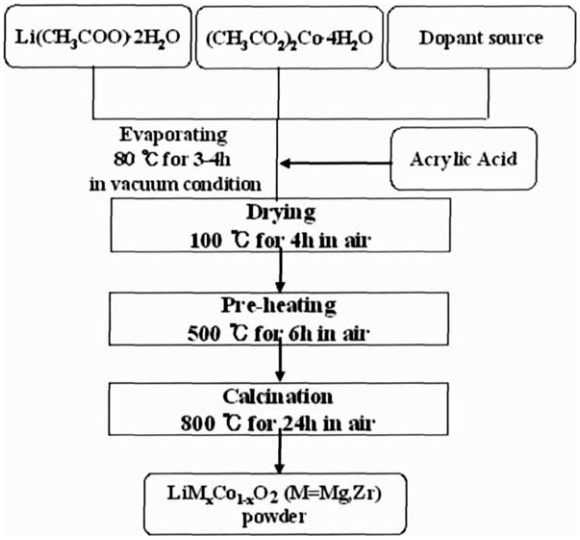

Fig. 2. Experimental procedure for synthesis of $LiM_xCo_{1-x}O_2$ (M = Mg, Zr) powders by sol–gel process.

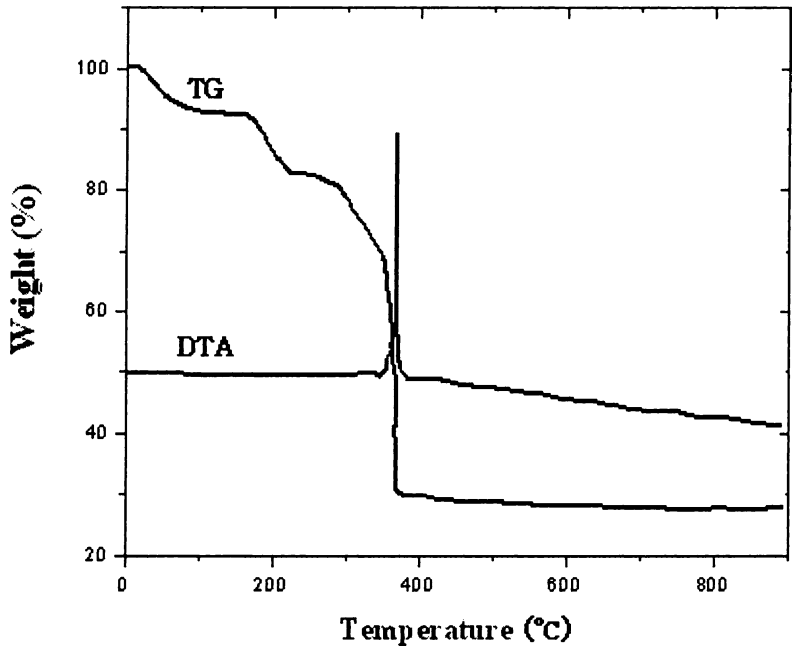

Fig. 3. TGA and DTA curves of $LiCoO_2$ gel precursor at heating rate of 2 °C per min and air flow rate of 100 cm^3 per min.

can increase the velocity of the electron. Polyvinylidenefluoride (PVDF) [13 wt.% in l-methyl-2-pyrrolinone (NMP)] was used as the binder. The active material, the conductive material and the binder in a ratio of 84:10:6 wt.% were mixed with an appropriate amount of acetone in a homogenizer at 5000 rpm. The slurry was cast on an A1 foil by means of the doctor blade method. The thickness of the sheet was adjusted around 100 μm by a rolling press. The prepared cathode was cut into 2 cm × 2 cm sample and dried at 80 °C in an oven for 24 h.

The battery was assembled in a dry room with less than 2% relative humidity. The anode was Li metal foil attached to a Cu grid. The electrolyte was 1 M $LiPF_6$ dissolved in ethylene carbonate (EC), ethyl methyl carbonate (EMC) and dimethyl carbonate (DMC) (1:1:1) and the separator was a polypropylene membrane (Celgard 2400).

The charge–discharge characteristics of the cells were galvanostatically tested by means of a battery cycler (Won A Tech., WBC 3000) at a specific current of C/5. The voltage ranges of charge and discharge were 3–4.3 V and 3–4.5 V,

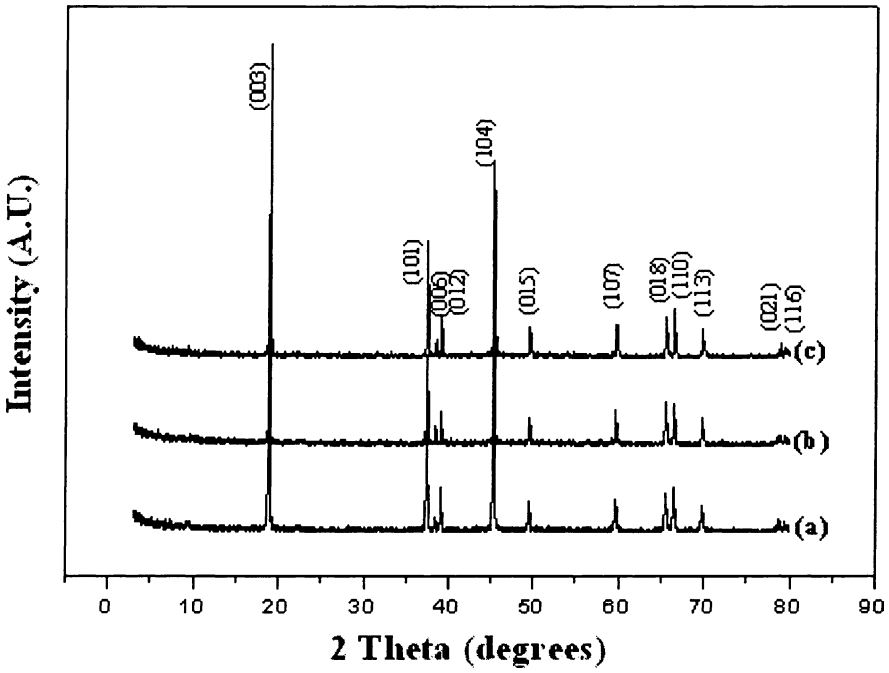

Fig. 4. XRD patterns of (a) $LiCoO_2$, (b) $LiMg_{0.01}Co_{0.99}O_2$, (c) $LiZr_{0.01}Co_{0.99}O_2$ powder calcined at 800 °C.

respectively. A rest time of 15 min was included to enable electrochemical equilibrium to be reached.

3. Results and discussion

3.1. TGA/DTA curves

The gel precursor was the intermediate product obtained on the way to synthesizing $LiCoO_2$ by the sol–gel method. The thermal behaviour of the gel precursor has been found [15] to determine the process condition, the crystallinity of the powder, the particle size, the lattice constant, and the specific surface-area. Accordingly, the thermal behaviour was analyzed by thermogravimetric analysis (TGA) and differential thermal analysis (DTA) (Figs. 1 and 2).

The TGA/DTA curves for the $LiCoO_2$ gel precursor obtained from lithium acetate and cobalt acetate with acrylic acid as a chelating agent are presented in Fig. 3. A weight loss of 20% occurs initially until 250 °C, and an additional decrease of 70% is observed until 400 °C. The initial decrease is due to the thermal decomposition of solvent, acetate and acrylic acid [16]. The secondary weight loss is due to the thermal decomposition between carbon and oxygen of the acrylic acid [17]. There is no weight loss over 600 °C.

Given the above findings, the gel precursor must be heated above 600 °C to obtain $LiCoO_2$ powder. The gel was calcined primarily at 500 °C and calcined again at 600 °C because 70% of the weight was lost below 400 °C. LT-$LiCoO_2$ (low temperature) and HT-$LiCoO_2$ (high temperature) are formed according to the calcination temperature. In the structure of HT-$LiCoO_2$, Li^+ and Co^{3+} ions occupy alternating (1 1 1) layers of octahedral sites in a cubic, close-packed, oxygen sub-lattice. It has a distorted rock-salt α-$NaFeO_2$ structure [18,19].

LT-$LiCoO_2$ has a different structure from HT-$LiCoO_2$ due to the decrease of the crystallinity [20,21]. There are also differences in electrochemical characteristics. The Li^+ intercalation–deintercalation of LT-$LiCoO_2$ occurrs at lower voltages than that of HT-$LiCoO_2$. The heat-treatment temperature is above 800 °C to obtain the structure of HT-$LiCoO_2$. The primary calcination temperature condition is 500 °C for 6 h, and the secondary calcination is conducted at 800 and 900 °C for 24 h.

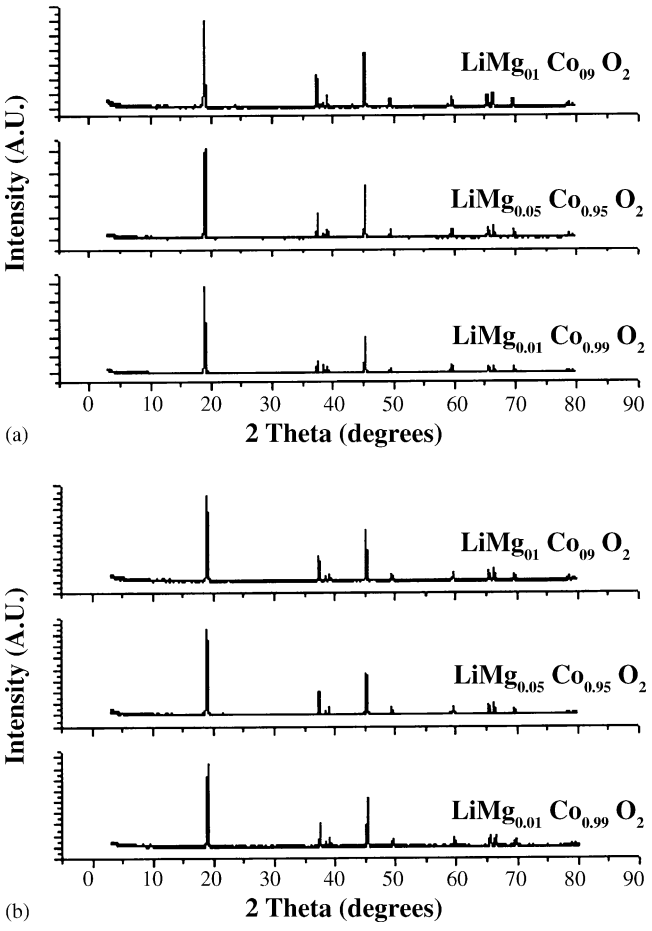

Fig. 5. XRD patterns of $LiMg_xCo_{1-x}O_2$(x = 0.01. 0.05, 0.1) powder calcined at (a) 800 °C and (b) 900 °C.

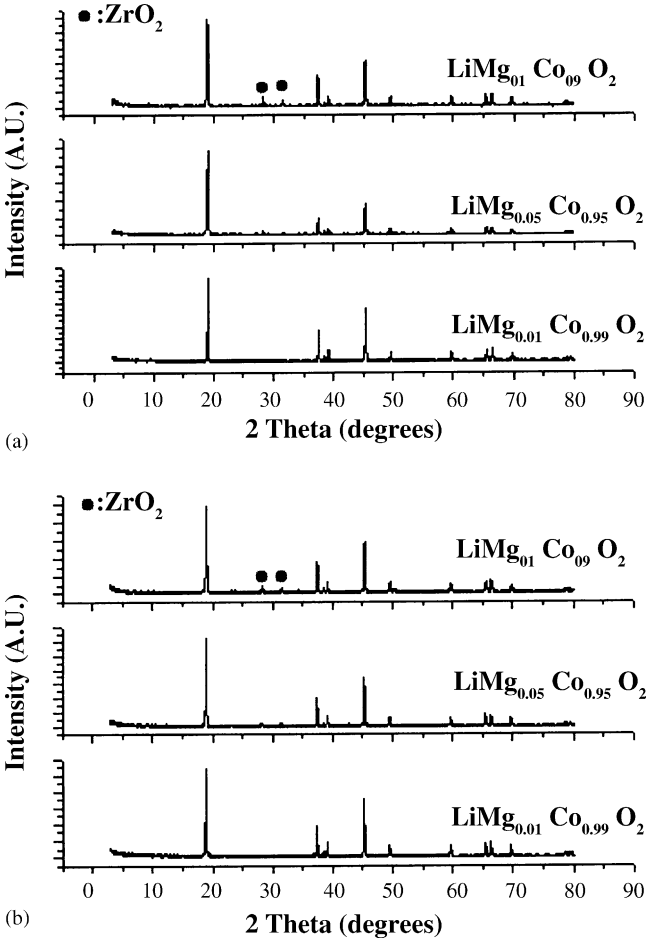

Fig. 6. XRD patterns of $LiZr_xCo_{1-x}O_2$ (x = 0.01, 0.05, 0.1) powder calcined at (a) 800 °C and (b) 900 °C.

3.2. X-ray diffraction

The XRD patterns of bare-$LiCoO_2$, $LiMg_{0.01}Co_{0.99}O_2$ and $LiZr_{0.01}Co_{0.99}O_2$ powder calcined at 800 °C for 24 h are presented in Fig. 4. The peaks are located at $2\theta = 19°$, 36°, and 44°. This is the crystal structure of the rhombohedral unit cell ($R\bar{3}m$ space group) in a hexagonal system, and the layered structure of the α-$NaFeO_2$ type found in a typical $LiMO_2$ oxide. The materials are HT-$LiCoO_2$ type because the (0 0 6), (1 0 2) peaks and the (1 0 8), (1 1 0) peaks are well separated.

The XRD patterns for $LiMg_xCo_{1-x}O_2$ (x = 0.01, 0.05, 0.1) powder calcined at 800 and 900 °C are given in Fig. 5. There are no impurity peaks at $0 \leq x \leq 0.1$. The XRD patterns for $LiZr_xCoi_{1-x}O_2$ (x = 0.01, 0.05, 0.1) powder calcined at 800 and 900 °C are shown in Fig. 6. There are impurity peaks of ZrO_2 at x = 0.1.

The lattice constants of $LiMg_xCo_{1-x}O_2$ and $LiZr_xCo_{1-x}O_2$ powders are given Fig. 7. The lattice parameters of axis a and c were calculated by means of the least-squares method and assuming hexagonal settings. The doping of Mg or Zr causes changes in the lattice parameters. As the concentration of doping materials increases, the lattice parameters a and c increase. These phenomena can be explained in terms of the ion sizes of Co^{3+}, Mg^{2+}, and Zr^{4+}. When the atoms have ionic bonding with 6-coordination, the sizes of the ions are 0.76 Å (Li^+), 0.64 Å (Co^{2+}), 0.545 Å (Co^{3+}), 0.72 Å (Mg^{2+}), and 0.72 Å (Zr^{4+}) [22]. The sizes of Mg^{2+} and Zr^{4+} are close to that of Li^+, but are larger than those of Co^{2+} and Co^{3+}. If the lattice parameters are increased by the addition of Mg^{2+} and Zr^{4+}, then it could be assumed that the doped ions substituted for Co^{2+} and Co^{3+} in the cobalt layer.

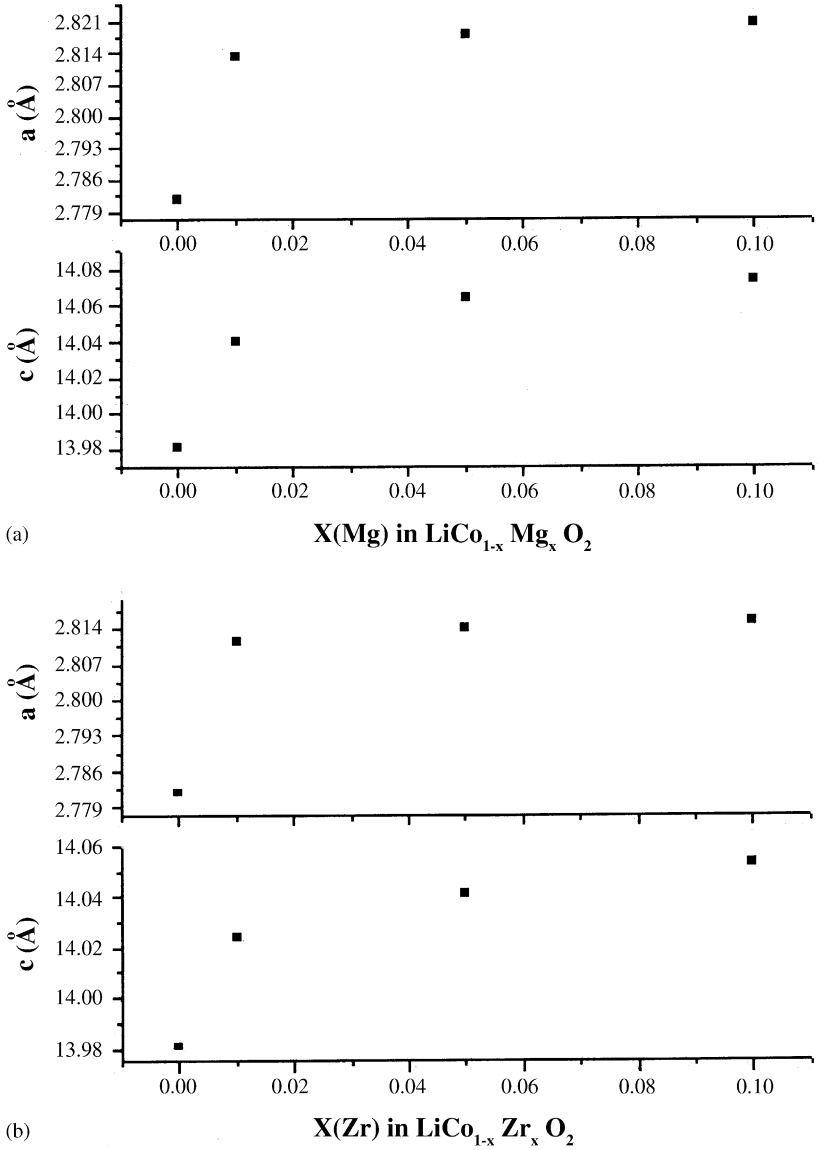

Fig. 7. Structural parameters of (a) $LiMg_xCo_{1-x}O_2$ and (b) $LiZr_xCo_{1-x}O_2$ powders.

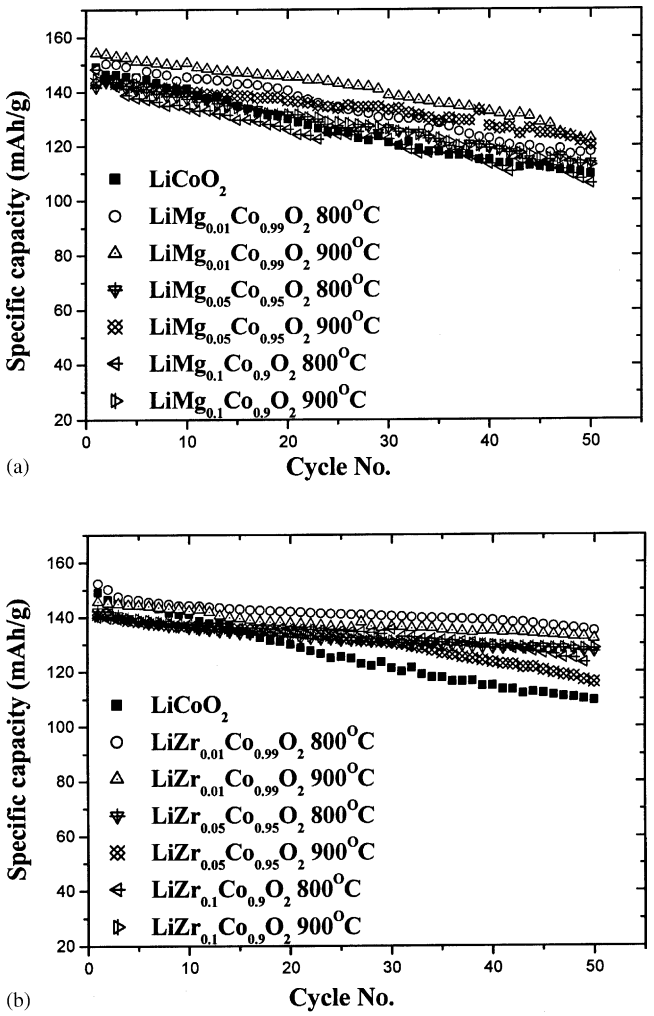

Fig. 8. Cycling performances of (a) bare-$LiCoO_2$ and Mg doped-$LiCoO_2$ and (b) Zr doped-$LiCoO_2$ calcined at 800 and 900 °C (voltage range: 3–4.3 V).

3.3. Charge–discharge characteristics

Changes in discharge capacity with cycling were measured in the voltage range of 3.0–4.3 V and 3.0–4.5 V, respectively. The cycling performance of bare-$LiCoO_2$ and Mg doped-$LiCoO_2$ calcined at 800 and 900 °C in the voltage range of 3.0–4.3 V is given in Fig. 8(a). The initial discharge capacity of $LiMg_{0.01}Co_{0.99}O_2$ calcined at 900 °C for 24 h and bare-$LiCoO_2$ calcined at 800 °C for 24 h is 154.27 and 149.13 mAh g^{-1}, respectively. When calcined at 800 °C for 24 h, the former material gave an initial discharge capacity of 148.52 mAh g^{-1}. When the amount of dopant is increased to 0.05 and 0.1 M, the initial discharge capacity is lower than that of bare-$LiCoC_2$. The cycling performance of bare-$LiCoO_2$ and Zr doped-$LiCoO_2$ calcined at 800 and 900 °C in the voltage range 3.0–4.3 V is shown in Fig. 8(b). The initial discharge capacity of the later material calcined at 800 °C is 153 mAh g^{-1}. As the heat temperature and the dopant amount increase, however, the initial discharge capacity decrease.

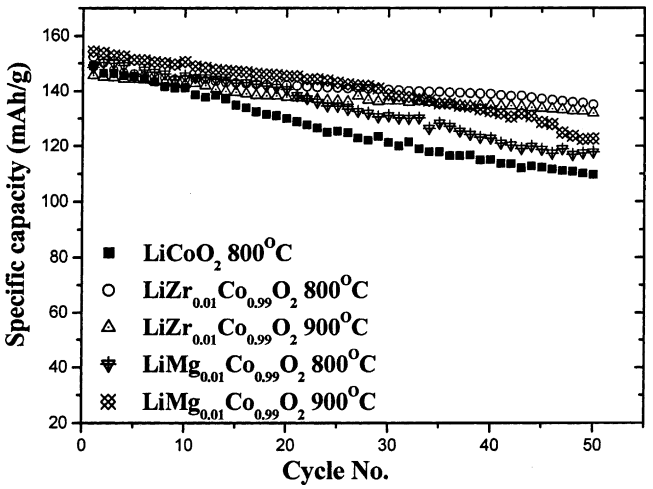

Fig. 9. Cycling performances of $LiCoO_2$, $LiMg_{0.01}Co_{0.99}O_2$ and $LiZr_{0.01}Co_{0.99}O_2$ calcined at 800 and 900 °C (voltage range: 3–4.3 V).

The cycling performance of bare-$LiCoO_2$, $LiMg_{0.01}Co_{0.99}O_2$ and $LiZr_{0.01}Co_{0.99}O_2$ calcined at 800 and 900 °C in the voltage range of 3.0–4.3 V is presented in Fig. 9. The discharge capacities of the three electrodes are initially very similar, but differences develop as cycling progresses. $LiMg_{0.01}Co_{0.99}O_2$ exhibits slightly higher discharge capacity than bare-$LiCoO_2$, but the rates at which the capacities decrease are very close. $LiZr_{0.01}Co_{0.99}O_2$ yields a similar initial discharge capacity to bare-$LiCoO_2$ and $LiMg_{0.01}Co_{0.99}O_2$. On further cycling, however, the capacity of $LiZr_{0.01}Co_{0.99}O_2$ maintains a steady value. After 50 cycles, the difference in the capacity of $LiZr_{0.01}Co_{0.99}O_2$ and bare-$LiCoO_2$ is 30 mAh g^{-1}. When the voltage range increases to 4.5 V, the difference becomes larger.

The cycling performances of bare-$LiCoO_2$, Mg doped-$LiCoO_2$ calcined at 900 °C and Zr doped-$LiCoO_2$ calcined at 800 °C in the voltage range of 3.0–4.5 V are shown in Fig. 10. The overall cycling performances are not superior to those found for the 4.3 V range. As the charge voltage increases, the amount of de-intercalated Li ions increases and the structural decay of $LiCoO_2$ becomes severe. When the dopants are added to the active material, the discharge capacity does not decrease severely. But, as the concentration of dopant increases, the initial capacity and the cycling performance become worse.

The cycling performances of bare-$LiCoO_2$, $LiMg_{0.01}Co_{0.99}O_2$, and $LiZr_{0.01}Co_{0.99}O_2$ in the voltage range of 3.0–4.5 V are given in Fig. 11. The initial discharge capacities are 190.5, 191.91, and 194.95 mAh g^{-1} for bare-$LiCoO_2$, $LiZr_{0.01}Co_{0.99}O_2$, and $LiZr_{0.01}Co_{0.99}O_2$, respectively. After 50 cycles, the capacity of bare-$LiCoO_2$ is 113.8 mAh g^{-1}, which is a 40% decrease. By contrast, the corresponding capacity of $LiMg_{0.01}Co_{0.99}O_2$ is 155.91 mAh g^{-1} and that of $LiZr_{0.01}Co_{0.99}O_2$ is 162 mAh g^{-1}. These values represent only a 20% decrease of the initial values, so the addition of dopant increases the stability of the structure.

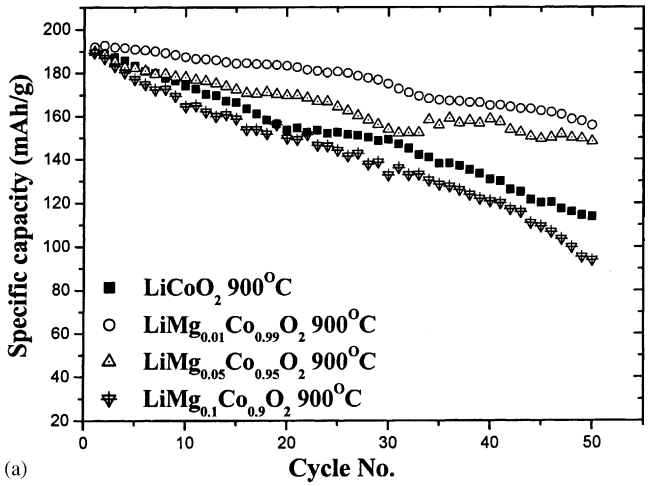

(a)

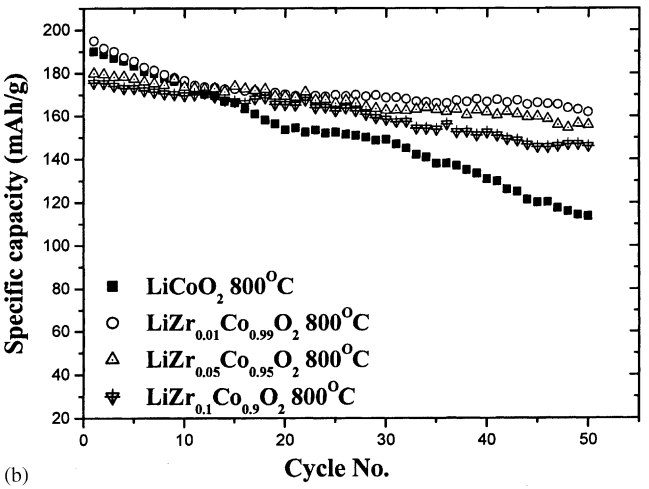

(b)

Fig. 10. Cycling performances of (a) bare-$LiCoO_2$ and Mg doped-$LiCoO_2$ calcined at 900 °C, (b) Zr doped-$LiCoO_2$ calcined at 800 °C (voltage range: 3–4.5 V).

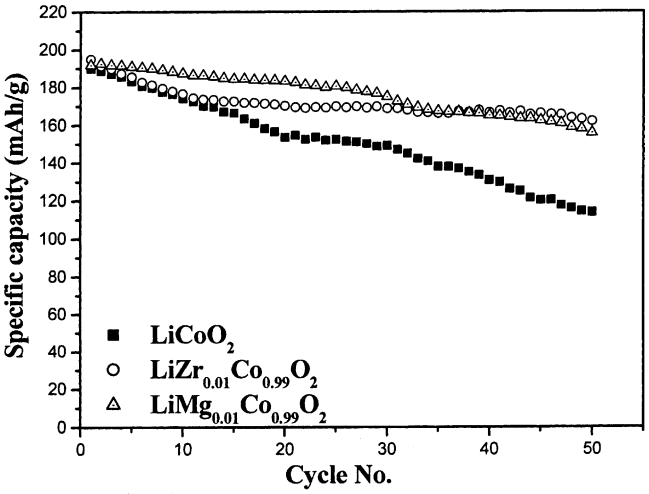

Fig. 11. Cycling performances of $LiCoO_2$, $LiMg_{0.01}Co_{0.99}O_2$ and $LiZr_{0.01}Co_{0.99}O_2$ (voltage range: 3–4.5 V).

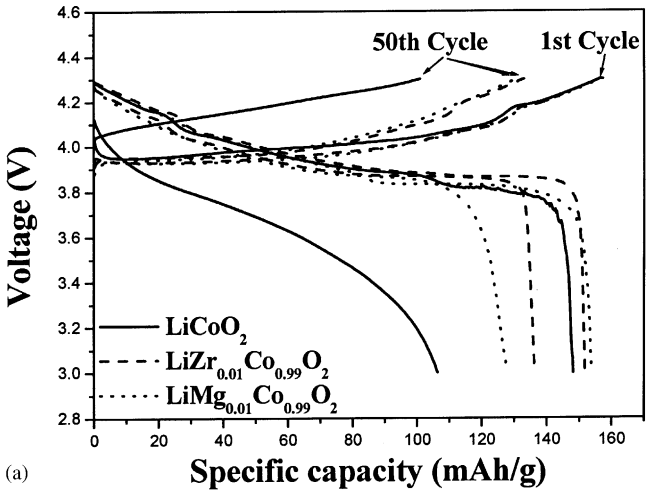

(a)

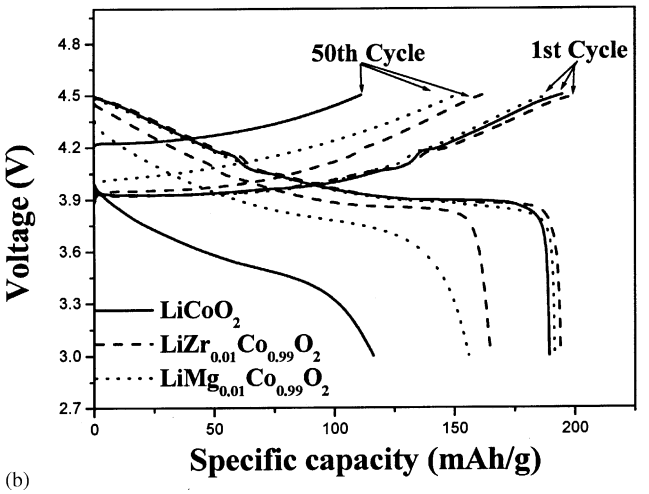

(b)

Fig. 12. Charge and discharge curves of $LiCoO_2$, $LiMg_{0.01}Co_{0.99}O_2$ and $LiZr_{0.01}Co_{0.99}O_2$ (voltage range: (a) 3–4.3 V, (b) 3–4.5 V).

The first and the last charge–discharge voltage curves of bare-$LiCoO_2$, $LiMg_{0.01}Co_{0.99}O_2$ and $LiZr_{0.01}Co_{0.99}O_2$ are shown in Fig. 12. The last curve of doped-$LiCoO_2$ indicates a decrease in discharge capacity, but the average working voltage is very similar to that of initial curve. This may be due to the improved structural stability with the addition of dopant. In case of bare-$LiCoO_2$, however, the charge–discharge capacity and the average working voltage decrease rapidly. The over intercalation–de-intercalation reaction of Li ions causes collapse of the $LiCoO_2$ structure and this eventually result in an increse in the internal resistance of the cell. Thus, the overall discharge capacity decreases rapidly.

De-intercalation of Li^+ ions occurs during charging of $LiCoO_2$, and vacant ordering phenomena occur due to depletion of Li^+ ions in the Li layer. In order to fill the vacant sites, Co^{4+} ions in the Co layer moves to the inter-slab space. Co^{4+} in inter-slab space increases the stability of the hexagonal structure of $LiCoO_2$, and prevents the phase transformation of monoclinic to hexagonal structure. The ion diameter of Co^{4+} in the inter-slab space is different from that of Li^+ ion.

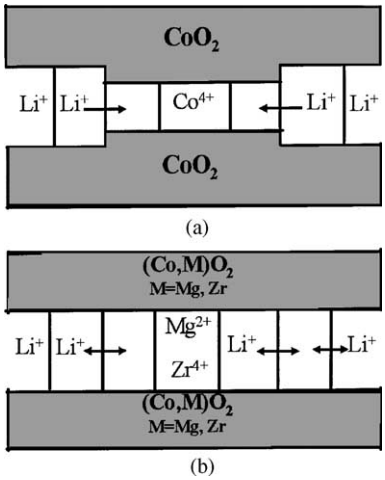

Fig. 13. Schematic representation of inter-slab space in (a) $LiCoO_2$ system and (b) $LiM_xCo_{1-x}O_2$ (M = Mg, Zr) system.

Therefore, the polarization of the cell increases due to the disturbance of Li^+ ion transportation during charge and discharge. These phenomena become severe over 4.2 V where Li is deintercalated over 0.5 mol. The other reason for the capacity decrease is that the cobalt dissolves due to the reaction between the electrolyte and the electrode [23]. Co^{4+} ions in the inter-slab space move to the surface of the electrode, along with the Li^+ ions during charge and discharge and dissolve in the electrolyte. Accordingly, the Co^{4+} ions in the inter-slab space becomes deficient. The Co ions in the Co-layer move to the inter-slab space in order to overcome the depletion of Co^{4+} ions and the polarization becomes severe.

Mg^{2+} or Zr^{4+} is doped into $LiCoO_2$ to solve the above problems. The Mg^{2+} or Zr^{4+} ions move to the inter-slab space along with Co^{4+} ions during the de-intercalation of Li+ ions over 4.2 V and they locate at the position of Li. The sizes of Mg^{2+} or Zr^{4+} are similar to that of the Li^+ ion and they assist the movement of Li^+ ions by preventing the vacancy ordering. This is called the 'pillaring effect', and is shown schematically in Fig. 13 [24].

The dopant ions move to the electrode surface and form a solid solution as charge and discharge continue. The solid solution acts as a coating layer and prevents the dissolution of Co^{4+} ions into the electrolyte. The structure becomes very stable during the phase transition and cycle stability is obtained over 4.2 V.

4. Conclusions

$LiCoO_2$ with a layered structure is manufactured by the sol–gel method and it is used as a cathode active-material in lithium rechargeable batteries. In order to reduce the capacity decrease over 4.2 V, $LiM_xCo_{1-x}O_2$ (M = Mg, Zr) is manufactured by the sol–gel method. The electrochemical and the physical characteristics of the powders are examined. XRD analysis identifies a rock-salt type layered structure. The cycling performance of $LiCoO_2$ over 4.2 V show a rapid decrease in the capacity. This undesirable effect is attributed to micro-cracks and structural collapse due to the anisotropic structural change during the charge and discharge. $LiM_xCo_{1-x}O_2$ (M = Mg, Zr) displays stable cycling behaviour. The sizes of Mg^{2+} or Zr^{4+} are similar to that of Li^+ ion and they assist the movement of Li^+ ions by preventing vacancy ordering, which is called the pillaring effect. The solid solution formed by dopants acts as a coating layer to prevent cobalt dissolution and the structure becomes very stable during the phase transition. Thus, cycle stability is obtained.

Acknowledgements

The present work was partially supported by K-2000 program in KIST, and the 21st Century Frontier Research Program of CNMT in Korea.

References

[1] K. Mizushima, P.C. Jones, P.C. Wiseman, J.B. Goodenough, Mater. Res. Bull. 15 (1980) 783.
[2] T. Nagaura, K. Tozawa, Prog. Batt. Solar Cells (1991) 209.
[3] M. Anraya, J.R. Dahn, J.S. Preston, E. Rossen, J.N. Reimers, J. Electrochem. Soc. 140 (1993) 575.
[4] B. Wang, J.B. Bates, F.X. Hart, B.C. Sales, R.A. Zuhr, J.D. Robertson, J. Electrochem. Soc. 143 (1996) 3203.
[5] S.T. Myung, N. Kumagai, S. Komaba, H.T. Chung, Solid State Ionics 139 (2001) 47.
[6] Y.J. Kim, T.J. Kim, J.W. Shin, B. Park, J. Cho, J. Electrochem. Soc. 49 (10) (2002) A1337.
[7] J. Cho, C.S. Kim, S.I. Yoo, Electrochem. Solid-State Lett. 3 (8) (2000) 362.
[8] Z. Wang, C. Wu, L. Liu, F. Wu, L. Chen, X. Huang, J. Electrochem. Soc. 149 (2002) A466.
[9] Z. Chen, J.R. Dahn, Electrochem. Solid-State Lett. 5 (10) (2002) A213.
[10] I. Saadoune, C. Delmas, J. Solid State Chem. 136 (1998) 8.
[11] R. Stoyanova, E. Zhecheva, L. Zarkova, Solid State Ionics 73 (1994) 233.
[12] Y.-I. Jang, B. Huang, H. Wang, H. Tamura, J. Electrochem. Soc. 146 (1999) 862.
[13] R. Alcantare, P. Lavela, J.L. Tirado, J. Solid State Chenv. 134 (1997) 265.
[14] M. Mladenov, R. Stoyanova, E. Zhecheva, S. Vassilev, Electrochem. Commun. 3 (2001) 410.
[15] J. Desilvesrt, O. Haas, J. Electrochem. Soc. 137 (1990) 50.
[16] J.M. Tarascon, W.R. McKinnon, F. Coowar, T.N. Boowmr, G. Amatucci, D. Guyomard, J. Electrochem. Soc. 141 (1994) 1421.
[17] T. Ohzuku, M. Kitagawa, T. Hirai, J. Electrochem. Soc. 137 (1990) 769.
[18] H.J. Oman, P.J. Wiseman, Acta Cryst. C40 (1984) 12.
[19] J.N. Reimiers, J.R. Dahn, J. Electrochem. Soc. 139 (1992) 2091.
[20] E. Rossen, J.N. Reimers, J.R. Dahn, Solid State Ionics 62 (1993) 53.
[21] R.J. Gummow, M.M. Thackeray, W.I.F. David, S. Hull, Mater. Res. Bull. 27 (1992) 327.
[22] R.D. Shannon, C.T. Prewitt, Acta Crystallogr. B52 (1969) 925.
[23] G.G. Amatucci, J.M. Tarascon, L.C. Klein, Solid State Ionics 83 (1996) 167.
[24] C. Pouillerie, L. Crohuennec, P. Biensan, J. Electrochem. Soc. 147 (2000) 2061.